Macromolecules

pubs.acs.org/Macromolecules Article

A Tunable, Particle-Based Model for the Diverse Conformations Exhibited by Chiral Homopolymers

Natalie Buchanan, Joules Provenzano, and Poornima Padmanabhan*

Cite This: *Macromolecules* 2022, 55, 6321−6331 Read Online

ACCESS | Metrics & More | Article Recommendations

ABSTRACT: Chiral block copolymers capable of hierarchical self-assembly can also exhibit chirality transfer—the transfer of chirality at the monomer or conformational scale to the self-assembly. Prior studies focused on experimental and theoretical methods that are unable to fully decouple the thermodynamic origins of chirality transfer and necessitate the development of particle-based models that can be used to quantify intrachain, interchain, and entropic contributions. With this goal in mind, in this work, we developed a parametrized coarse-grained model of a chiral homopolymer and extensively characterized the resulting conformations. Specifically, the energetic parameter in the angular and dihedral potentials, the angular set point, and the dihedral set point are systematically varied to produce a wide range of conformations from a random coil to a nearly ideal helix. The average helicity, pitch, persistence length, and end-to-end distance are measured, and correlations between the model parameters and resulting conformations are obtained. Using available experimental data on model polypeptoid-based chiral polymers, we back out the required parameters that produce similar pitch and persistence length ratios reported in the experiments. The conformations for the experimentally matched chains appear to be somewhat flexible, exhibiting some helical turns. Our model is versatile and can be used to perform molecular dynamics simulations of chiral block copolymers and even sequence-specific polypeptides to study their self-assembly and to gain thermodynamic insights.

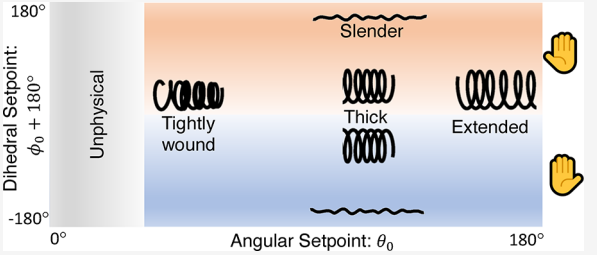

INTRODUCTION

Chirality, the ability to classify an object as either left-handed or right-handed, can be used to describe objects of a large span of length scales. In particular, by use of macromolecular building blocks, chirality can exhibit within the same system at several length scales simultaneously—beginning at an asymmetric tetrahedral carbon atom to the conformations (helical) of the macromolecule and culminating in the self-assembly of several macromolecules into chiral foldamers and microstructures. This phenomenon where chirality at a smaller length scale results in chirality at subsequently longer length scales is known as chirality transfer. Numerous examples of chirality transfer in systems of chiral small molecules, proteins, DNA, and polymers abound in the literature.[1−5]

Because chiral materials are known to exhibit novel optical properties, the ability to control and tune this phenomenon of chirality transfer alongside self-assembly can prove to be powerful for the synthesis of novel materials. One such example is the single gyroid that exhibits a negative refractive index and is found to occur in butterfly wing scales, imparting structural color.[6,7] These structures have since been synthesized via templating[7−9] and, more recently, by leveraging the self-assembly of a chiral polypeptide-based triblock copolymer.[10] Several other examples of chirality transfer in diblock copolymers where self-assembly plays a role include novel morphologies such as the helical phase,[11−16] twisted lamellae,[15] rosettes,[17] superhelices,[18] and toroids.[19] Other studies of polypeptoid-based chiral block copolymers show that chirality plays a role in the thermodynamics of self-assembly even for nonchiral self-assembled structures. Specifically, the nature of conformations—whether coil-like or helix-like—was shown to impact the location of the order−disorder transition,[11,20] the domain sizes of the cylinder phase,[21] and the windows of stability of specific thermodynamic phases.[22] Thus, the importance of the role of conformational chirality in self-assembly is evident, whether accompanied by chirality transfer or not.

Theoretical studies of chiral block copolymers using orientational self-consistent field theory[23−25] are helpful in delineating large regions in the phase diagram and predicting several chiral morphologies consistent with experiments. These studies have also put forth mechanistic explanations regarding geometric frustration that drives the stability of the helical phases. Despite these advances, the role of conformational

Received: March 25, 2022
Revised: June 8, 2022
Published: July 18, 2022

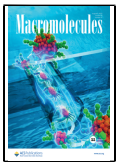

https://doi.org/10.1021/acs.macromol.2c00613
Macromolecules 2022, 55, 6321−6331

chirality on the thermodynamics and hierarchical self-assembly is not yet well understood. Particle-based simulations can be used to obtain conformational statistics and can decouple the roles of various thermodynamic driving forces such as intra- and intermolecular interactions or entropic contributions using free energy calculations.

Models for conformational chirality of polymers exist in the literature, but these were largely developed by keeping proteins and their secondary helical structures in mind, or for polymers in dilute solution. Atomistic models for polyalanine[26,27] using CHARMM-type[28] force fields account for detailed interactions such as hydrogen bonding and electrostatics but add significantly to computational cost. In coarse-grained models such as the MARTINI force field,[29,30] several atoms are mapped onto a coarse-grained bead, enabling an accurate description of chemical specificity while saving some computational cost. In block copolymers, because each block comprises identical monomers, intrablock interactions may be simplified further, and a minimal phenomenological model that captures the key conformational behavior ought to be sufficient.

Early attempts of modeling the conformational states in polypeptides[31] were based on the 1-D Ising model and focused on the coil−helix transition. More recently, Kemp and Chen proposed a wormlike polymer chain capable of chiral conformations based on directional interactions[32] for a fixed bond angle. Varshney et al.[33] developed a Monte Carlo model for wormlike polymers and utilized an energetic penalty when beads were outside the conformational prescription set by the angles and dihedrals. Boehm and Terentjev[34] utilized molecular dynamics simulations to model a chiral homopolymer in an implicit solvent, where the conformations spanned the helix, coil, and globule states. Williams and Bachmann[35] proposed another mode with angular and torsional potentials and produced a phase map of conformations by varying all the energetic coefficients of the torsional potential. Continuum models[36] with bending and torsional elasticity have been used to map conformational metrics such as the persistence length by using the tangent−tangent correlation and the binormal−binormal correlations, specifically developed for double-stranded DNA. Other useful conformational metrics such as pitch, diameter of the helical turn, and contour length can also be found from continuum models.[37] Overall, studies on the particle-based models showed that angular and dihedral potentials are necessary to drive chiral conformations, but most studies did not examine how the angular and dihedral set points affected the conformations.

Previous models are not specific enough to study block copolymers in the melt. Experimental characterization of polymer conformations[20,38] suggest that the conformational differences between chiral and achiral blocks may be subtle. This subtlety is missing in previous models which primarily focused on canonical conformations (helix, coil, and globule). Furthermore, polymer melts do not serve as bad solvents where the globular conformation is not generally relevant. In this work, we adopt potentials similar to those published in the literature and fully characterize the conformations so that a quantitative relationship between interaction potentials and conformations can be established, thereby resulting in a fully parametrizable and tunable model capable of modeling chiral homopolymers. Specifically, we examine how changing three parameters (θ_0, ϕ_0, $K_\phi = K_\theta$) affects the conformation of the helical chains. The conformation is quantified via pitch, persistence length, end-to-end distance, and helicity. The detailed characterization will enable selection of simulation parameters to further study the polymer thermodynamics relevant to the experimental block copolymers.

METHODOLOGY

Molecular dynamics simulations utilized in this work were performed by using LAMMPS[39] on computational resources provided by Research Computing at RIT.[40] The model for the chiral polymer is based on a minimal bead−spring model[41] capable of helical conformations, proposed by Boehm and Terentjev.[34] The nonbonded interactions in Boehm and Terentjev[34] are modeled by the full Lennard-Jones potential[42] to span conformations from random coil to globule, applicable when the implicit solvents are good and bad, respectively. We envision using our model in a melt of block copolymers, where the good solvent regime applies and where the globular conformations are not relevant. Therefore, we use the repulsive-only Weeks−Chandler−Andersen potential[43] to model nonbonded interactions. The WCA potential between particles labeled i and j is given by

$$E_{\text{nonbonded},ij} = \begin{cases} 4\epsilon\left[\left(\frac{\sigma}{r_{ij}}\right)^{12} - \left(\frac{\sigma}{r_{ij}}\right)^{6}\right] + \epsilon, & r < 2^{1/6}\sigma \\ 0, & r \geq 2^{1/6}\sigma \end{cases} \quad (1)$$

The choice of the WCA potential over the Lennard-Jones potential has been utilized extensively to model polymer melts and is thought to enhance sampling of polymer conformations.[41] Two commonly used bonded interaction potentials were used in this study to assess any qualitative differences between the two. First, we used the finite extensible nonlinear elastic (FENE) potential following the equation

$$E_{\text{FENE},ij} = -0.5K_{\text{FENE}}{R_0}^2 \ln\left[1 - \left(\frac{r_{ij}}{R_0}\right)^2\right] + 4\epsilon\left[\left(\frac{\sigma}{r_{ij}}\right)^{12} - \left(\frac{\sigma}{r_{ij}}\right)^{6}\right] + \epsilon \quad (2)$$

with $K_{\text{FENE}} = 30k_BT$ and $R_0 = 1.5\sigma$. Note that while R_0 is provided, the equilibrium bond length that minimizes the potential energy is approximately 0.97σ. Second, we used the harmonic potential for bonded interactions following the equation

$$E_{\text{har},ij} = K_{\text{har}}(r_{ij} - R_0)^2 \quad (3)$$

with $K_{\text{har}} = 400k_BT$ and $R_0 = 1.0\sigma$. The equilibrium bond length where the potential energy is minimized is R_0. The value of K_{har} was chosen so that the profile for E_{har} was approximately the same as when FENE bonds were implemented. We note that despite the typical use of the FENE model to study polymer melts, we generally find that chiral polymers are more dynamically stable with harmonic bonds. In the Results and Discussion section, we find that the choice of the bonded potential does not significantly impact the resulting conformations.

To drive chiral conformations, angular and dihedral potentials are necessary. Angles were modeled by using a harmonic potential. In LAMMPS, the harmonic potential is implemented through a quartic equation, where K_3 and K_4 are set to zero, to recover the harmonic equation. The parameter K_2 is termed K_θ from this point onward because it is the only nonzero K term in the angular potential.

https://doi.org/10.1021/acs.macromol.2c00613
Macromolecules 2022, 55, 6321−6331

$$E_{\text{angle},ijk} = K_2(\theta_{ijk} - \theta_0)^2 + K_3(\theta_{ijk} - \theta_0)^3 + K_4(\theta_{ijk} - \theta_0)^4 = K_\theta(\theta_{ijk} - \theta_0)^2 \quad (4)$$

where θ_{ijk} is the angle formed by three monomers with sequential indices i, j, and k. The set point θ_0 is also the equilibrium angle that minimizes potential energy.

The torsional forces are enforced on the chain by using dihedral bond potential of the Fourier form, truncated after the first cosine function.

$$E_{\text{dihedral},ijkl} = K_\phi[1 + \cos(\phi_{ijkl} - \phi_0)] \quad (5)$$

where K_ϕ is the energetic parameter and ϕ_{ijkl} is the dihedral angle formed by four monomers with sequential indices i, j, k, and l. The value of ϕ that minimizes the dihedral energy, also termed the dihedral set point, is $\phi_0 - 180°$ and not ϕ_0. When $\phi_0 = \pm 180°$, a coplanar arrangement of atoms with overlapping atoms is preferred. When $\phi_0 = 0°$, a coplanar arrangement of atoms in a zigzag pattern is preferred.

For simplicity in the overall model, we limit the number of variables by setting $K_\theta = K_\phi$. Henceforth, we will nondimensionalize this energy and refer to this parameter as $K^* = K/k_BT$. A single polymer molecule with $N = 100$ beads is simulated in an implicit solvent. The simulations are run in an NVT ensemble with $k_BT = 1.0$ by using the Nosé−Hoover thermostat, with a time step $\delta t = 0.0001$ and the thermostat damping parameter as 0.1τ for 30 million time steps. The box size is set to be very large relative to the size of the molecule. The atomic positions are initialized by placing atoms at the equilibrium bond length, angular, and dihedral values that would produce the energetically most favorable conformation to prevent initial stresses that might generate some angular momentum.

We vary θ_0, ϕ_0, and K^* and study how it affects the configuration of the chiral chain. We note that θ_0 and ϕ_0 are the set points that determine the conformations that minimize the energetic contributions from these terms. Physically, these are set by the steric repulsion of the side groups or torsional forces present in the polymer backbone. We characterize the chains using measurements of its conformation by using experimentally measurable quantities such as helicity, pitch, persistence length, and end-to-end distance. The measurements are obtained by averaging over the last 10% of time steps for each simulation. The details for these calculations are described alongside the results in the next section.

RESULTS AND DISCUSSION

Chain Characterization Metrics. We characterize the chiral chains using several metrics that are commonly measured during the experimental characterization of these polymers to bridge the gap between simulated and experimental systems. Figure 1 shows an illustration of the experimentally relevant metrics at the segmental scale and conformational scale. The resulting angles and dihedrals are given by θ and ϕ. The pitch p measures the average distance between monomers separated by a complete helical turn, the persistence length l_p measures the distance beyond which the helical axis orientation becomes uncorrelated, and the end-to-end distance R_{ee} measures the distance between the first and last monomer.

The methodology used to calculate the pitch and persistence length is shown in Figure 2. In these calculations, the index separation between monomers along the backbone is denoted

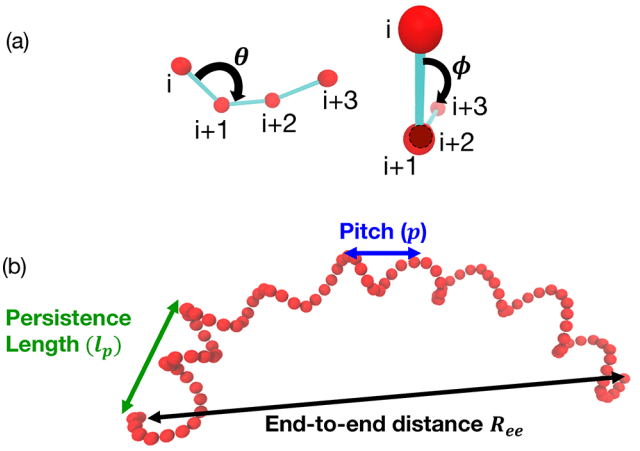

Figure 1. Illustration showing (a) measurements relevant at the segmental scale and (b) characterization methods at the conformational scale: end-to-end distance, pitch (height of helical turns), and persistence length.

by s. First, the average dot product of bond vectors $\vec{b}_i$ and $\vec{b}_{i+s}$ along the backbone, separated by s and averaged over indices i, is obtained. The average dot product starts at the maximum value of unity and exhibits oscillations with a decreasing amplitude, as evident in Figure 2a. The oscillations for small s are characteristic of the alignment of neighboring bonds, followed by antialignment, and further realignment at longer separations, when one helical turn is executed. Therefore, each peak corresponds to the completion of one helical turn (Figure 2a). Only the first peak is used to obtain an accurate estimate of the pitch because kinks or decorrelations may occur at longer distances along the backbone. The backbone separation at the first peak is thus identified as s_p.

In nonchiral polymers, the persistence length[44] is extracted from a plot similar to Figure 2a, where the bond orientation function exhibits an exponential decay. In chiral polymers, one has to instead examine the decorrelation of several helical turns. Therefore, the length scale over which the amplitude decays will give a measure of the persistence length. In Figure 2b, we plot the logarithm of the peak values in Figure 2a, denoted by diamond symbols, versus monomer separation s. The data are fitted to a straight line by using the equation

$$\ln(\text{peak}\langle \vec{b}_i \cdot \vec{b}_{i+s} \rangle) = \frac{-s}{s_l} + c \quad (6)$$

from which the value of s_l can be extracted. This value s_l corresponds to the backbone separation at which the helical turns decorrelate. We note that for very small values of K^* the angular and dihedral potentials do not contribute significantly, and the average dot product decorrelates rapidly, within 2−4 monomer index separations, suggesting a random coil conformation. For this reason, pitch and persistence length calculations using eq 6 are performed only for $K^* \geq 2$. For $K^* < 2$, the persistence length is computed from the decay of the dot product directly instead of from the peaks.

Finally, we compute the physical distances between monomers separated by s along the backbone in Figure 2c. The distances corresponding to the previously identified values of s_p from Figure 2a and s_l from Figure 2b are the pitch p and persistence length l_p, respectively. Another important order parameter to quantify the chiral conformations of the chains is helicity, h. We define helicity as the fraction of residues closely

https://doi.org/10.1021/acs.macromol.2c00613
Macromolecules 2022, 55, 6321−6331

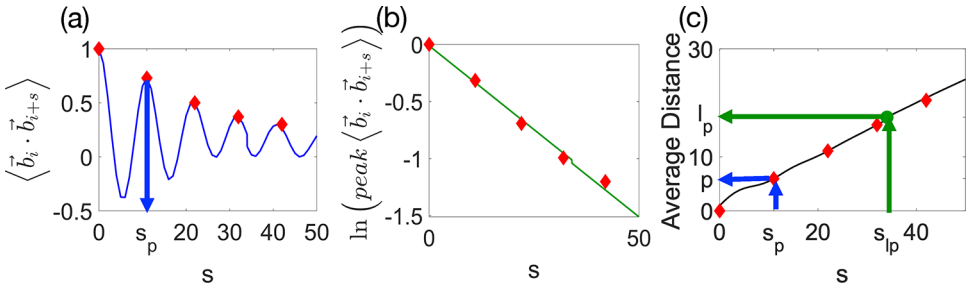

Figure 2. Sample data showing the analysis to compute pitch and persistence length. (a) Bond orientation function with the peaks shown as red diamonds. (b) Exponential fit to the peaks of the tangent function. The value of s_p is extracted from the equation. (c) Pitch (blue) extracted from average distance by finding the average distance where $s = s_p$ from the first tangent peak. l_p (green) is extracted by finding the average distance where $s = s_{lp}$.

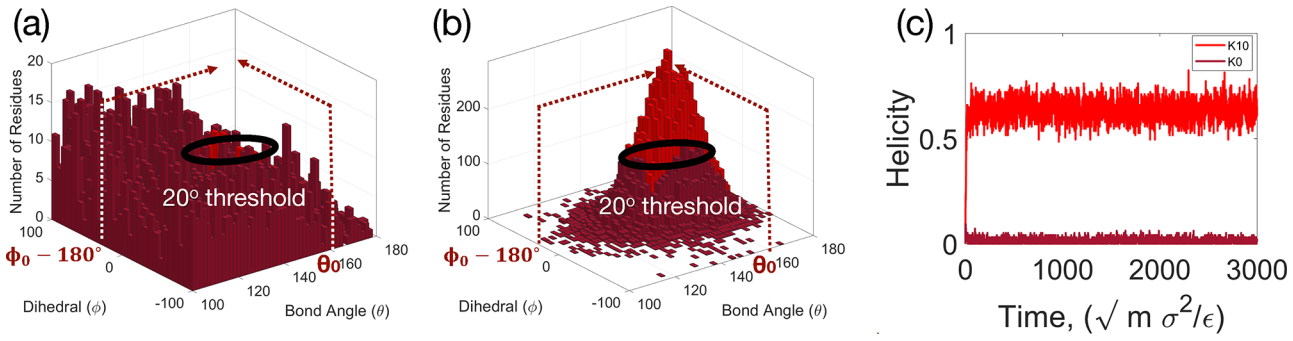

Figure 3. Demonstration of the helicity calculation using the distribution of angles and dihedrals. (a) and (b) show the distribution of angles and dihedrals for the last 10% time steps. For each time step, the fraction of residues that are within the threshold (bright red) is the value of helicity. (a) Data of a random coil ($K^* = 0$, $\theta_0 = 160°$, and $\phi_0 = 200°$). (b) Data from a helix ($K^* = 10$, $\theta_0 = 160°$, and $\phi_0 = 200°$). (c) Helicity measurements over time for the random coil and the helix.

following the set points. This metric has been used in several studies previously,[33,34] and we use the following equation:

$$h = \frac{r}{N-2} \tag{7}$$

where h is the helicity represented as a fraction between 0 and 1, r is the number of helical residues corresponding to the helicity criterion, and N is the total number of beads in the chain. A residue is a set of four atoms for which one can define a dihedral. The associated angle is defined for the first three atoms. A residue is considered helical if both the angle and dihedral are within a specified tolerance of the angular and dihedral set points, θ_0 and $\phi_0 - 180°$, respectively. The tolerance threshold is set to 20°, following previous literature.[34,45] In other words, r equals the number of residues with $\theta \in [\theta_0 - 20°, \theta_0 + 20°]$ and $\phi \in [\phi_0 - 180° - 20°, \phi_0 - 180° + 20°]$.

A random coil is expected to have a low helicity whereas a perfect helix is expected to have a helicity of 1. Because of thermal fluctuations, the value of unity is never reached for the parameters selected in this study. The angular and dihedral distribution for each residue over 100 conformations is shown for a typical random coil (Figure 3a) and for a typical helix (Figure 3b). The distribution is shown in bright red for values that meet the criterion and in deep red for values that do not meet the criterion. The helicity is then computed by using eq 7. Figure 3c shows the helicity over time, from which the last 10% of data points is extracted and used to calculate an average value $\langle h \rangle = 0.636$ for the helical chain (bright red) and $\langle h \rangle = 0.014$ for the random coil (dark red).

Our final conformational metric is the mean-square end-to-end distance $\langle R_{ee}^2 \rangle$ obtained as the time average of the square of the end-to-end distance divided by the length of the chain N. Values for pitch, persistence length, and helicity combined with the end-to-end distance provide a detailed quantitative picture of the chain conformation, even though they may be correlated to one another. We now vary our model parameters K^*, θ_0, and ϕ_0 and assess their effect on chain conformations.

Effect of θ_0 on Chain Conformations. The angle formed by three monomers is set by the set point θ_0 because the value of the set point minimizes the angular potential energy. We varied θ_0 from 80° to 180° and fixed $\phi_0 - 180° = 20°$ and $K^* = 10$. Smaller values would lead to bead overlap of the first and third bead, resulting in unphysical conformations, and larger values would exceed the maximum polar angle.

Figure 4 shows visualizations of chains with select θ_0 values, from which it is apparent that the set point θ_0 is found to control the number of monomers per helical turn. At low θ_0, the coils are very short and very tightly wound (Figure 4a). As θ_0 increases, the coils have more monomers per helical turn and are therefore more loosely coiled (Figure 4b). When $\theta_0 = 180°$, the coils are fairly stretched out with many monomers per turn. In Table 1, the average number of monomers per helical turn is quantitatively shown, which follows the trend for the internal angle equation for two-dimensional s_p-sided planar polygons, $s_p = \frac{360°}{180° - \theta_0}$. This calculation is approximate due to two reasons. First, because of thermal noise, the bond angles will not precisely follow the set point θ_0. Second, in three dimensions, one will have to replace θ_0 with the projection of the bond angle onto the plane; nevertheless, it is apparent that

https://doi.org/10.1021/acs.macromol.2c00613
Macromolecules 2022, 55, 6321−6331

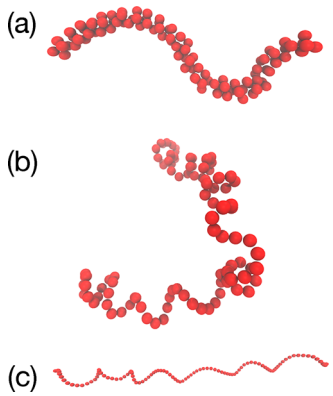

Figure 4. Visualizations of select polymer chains with increasing values of θ_0 with a constant value of $K^* = 10$ and $\phi_0 = 200°$. (a) $\theta_0 = 80°$, (b) $\theta_0 = 140°$, and (c) $\theta_0 = 180°$.

Table 1. Angular Set Point θ_0 vs Average Number of Monomers per Helical Turn s_p, Averaged over the Last 10% of the Simulation, for $K^* = 10$

	no. of monomers $\langle s_p \rangle$	
set point θ_0 (deg)	FENE	harmonic
80	4	4
100	4.22	4.33
120	5.86	5.77
140	7.71	7.833
160	11.24	11.23
180	14.82	13.13

as θ_0 increases, the number of monomers per turn also increases.

That θ_0 primarily controls the number of monomers per helical turn is also apparent via other quantitative chain metrics shown in Figure 5. The change in conformation is not captured in the helicity (Figure 5a) since helicity measures the proximity to the set points; here, by changing θ_0, the set point is itself changing. The persistence length (Figure 5b) increases as θ_0 increases, showing that the helical chain becomes more rodlike. Because of the increasing number of monomers per turn but fixed bond lengths, the pitch also increases (Figure 5c). The increases in pitch and persistence length are reflected by an increasing $\langle R_{ee}^2 \rangle$ (Figure 5d). Finally, we note that there appears to be no significant differences between the type of bonds used on the conformational metrics.

Effect of ϕ_0 on Chain Conformations. Next, we examined the effect of changing the dihedral set point while fixing $\theta_0 = 160°$ and $K^* = 10$. Notably, the sign of the dihedral angle set point $\phi_0 - 180°$ defines the overall handedness of the polymer chains even though specific regions within the chain could exhibit variations. To quantitatively identify the handedness of a single chain, the values of ϕ are measured and plotted in Figure 6a for three different set points. When $\phi_0 - 180° > 0$, most values of ϕ are found to be predominantly positive (Figure 6a) with above 75% of the residues having $\phi - 180° \geq 5°$. This results in the overall chain exhibiting left-handed chirality (Figure 6b). When $\phi_0 - 180° < 0$, the chain instead has a right-handed chirality where above 75% of the residues have $\phi \leq -5°$ (Figure 6d). For the special case of the set point $\phi_0 - 180° = 0$, we note that the dihedral angles are distributed equally between right-handed and left-handed values. Furthermore, we observe clusters or coils of right-handed and left-handed regions within the chain as shown in Figure 6c and describe this behavior as having mixed handedness rather than no handedness because the helicity values are high (not shown). In contrast, in a random coil formed at $K^* = 0$, an equal proportion of right-handed and left-handed dihedral angles combined with a low helicity suggests no handedness in the chain. Thus, only quantifying the proportion of left-handed or right-handed segmental ϕ is not

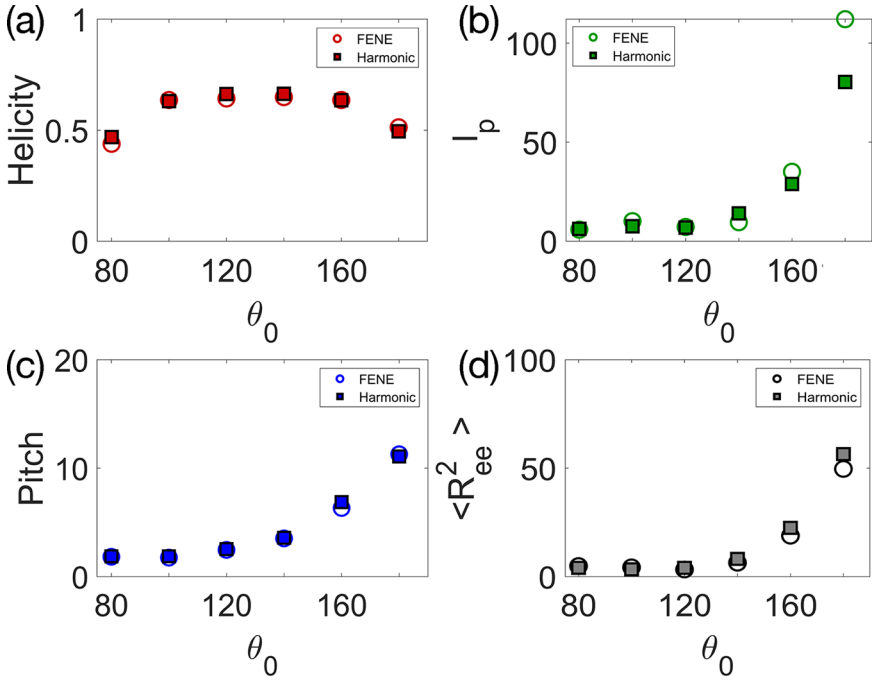

Figure 5. Chain characterization changing with θ_0 for $K^* = 10$ and $\phi_0 = 200°$: (a) helicity, (b) persistence length, (c) pitch, and (d) mean-square end-to-end distance normalized over N.

https://doi.org/10.1021/acs.macromol.2c00613
Macromolecules 2022, 55, 6321−6331

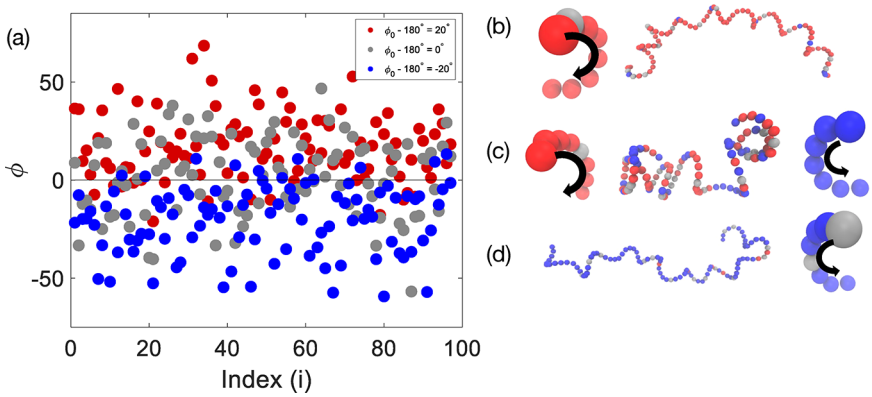

Figure 6. Effect of $\phi_0 - 180°$ on the handedness of the polymer chain. (a) Measured ϕ of each dihedral for chains with different handedness with $K^* = 10$ and $\theta_0 = 160°$. (b–d) Chains from (a) with select single turns are shown to demonstrate handedness. Colors indicate dihedral values where red = $\phi - 180° > 5°$, gray = $-5° \leq \phi - 180° \leq 5°$, and blue = $\phi - 180° < -5°$, (b) $\phi_0 - 180° = 20°$, (c) $\phi_0 - 180° = 0°$, and (d) $\phi_0 - 180° = -20°$.

sufficient in determining whether the chain is chiral; the distribution of ϕ and θ must be sharply peaked to produce high helicity (similar to Figure 3b), h, and for the chain to exhibit handedness.

Understanding the role of the dihedral set point ϕ_0 can be leveraged for a whole variety of chiral polymers. By changing the sign of $\phi_0 - 180°$, one can model different enantiomers of the same polymer. Furthermore, by varying the set points of ϕ_0 for each residue within the polymer, one can easily model polymers with specific chemical sequences. The overall handedness of the conformation in sequence-varied chiral polymers can still be quantified by the fraction of residues with $\phi > 0$.

Next, we examine the effect of the magnitude of $|\phi_0 - 180°|$ on the conformational metrics such as pitch and persistence length. From the snapshots in Figure 7, as $|\phi_0 - 180°|$ increases, the chains follow extended conformations with narrower widths of the helical turn.

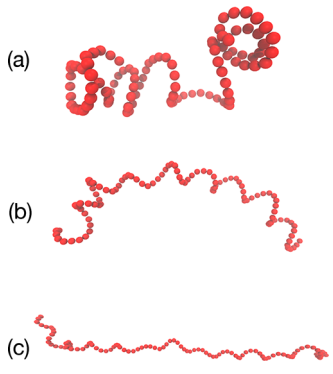

Figure 7. Snapshots from last time step of chains with increasing ϕ_0 with $K^* = 10$ and $\theta_0 = 160°$: (a) $\phi_0 - 180° = 0°$, (b) $\phi_0 - 180° = 20°$, and (c) $\phi_0 - 180° = 40°$.

Quantitative data for the effect of varying ϕ_0 on all the conformational metrics are shown in Figure 8. The chain conformation is not captured in the helicity values (Figure 8a) because by changing ϕ_0, we are again changing the set point itself. The increased rodlike behavior visually observed in Figure 7 is captured in the persistence length curve (Figure 8b). Further increase in $|\phi_0 - 180°|$ would result in a zigzag-like arrangement of atoms. The pitch, plotted in Figure 8c, shows nearly no dependence on ϕ_0. To understand this behavior, we provide the number of monomers per helical turn in Table 2. Recall that when $\phi_0 - 180° = 0°$, a coplanar arrangement of atoms is preferred, so the number of monomers per turn is related to the number of polygonal sides with angle θ_0. As $|\phi_0 - 180°|$ increases, the atoms are no longer coplanar, and the projection of the angle changes. Fewer monomers per turn are required to obtain two parallel vectors. This becomes apparent in considering an extreme case of $\phi_0 - 180° = 180°$, where an exact zigzag-like pattern will result in $s_p = 2$, or only two monomers per turn. Concomitantly, increasing $|\phi_0 - 180°|$ also increases the distance between monomers labeled i and $i + 3$. Overall, the net effect of fewer monomers per turn with larger distance between monomers i and $i + 3$ is that pitch is nearly independent of $|\phi_0 - 180°|$. This is accompanied by a smaller width of the helical turns (consistent with visual observations in Figure 7a–c).

Therefore, we note that the mechanisms for higher persistence lengths are entirely different when changing θ_0 or ϕ_0. By increasing the angular set point θ_0, an increase in monomers per turn occurs, which increases both pitch and persistence length. By increasing the magnitude of the dihedral set point $|\phi_0 - 180°|$, a decrease in monomers per turn combined with larger spacing results in near similar pitch but higher persistence lengths. Finally, the normalized end-to-end distance plotted in Figure 8d shows an increase, correlated to an increasing persistence length.

Effect of K^* on Chain Conformations. To study the effect of K^* on the chain conformations, we set $\theta_0 = 160°$ and $\phi_0 = 200°$. We increased K^* from 0 to 10.

As seen in the visualizations shown in Figure 9b–e, at low K^*, the chain behaves like a random coil because θ and ϕ have no effect on the interaction potential. As K^* increases, the chain appears to have more well-defined coils. This is also captured by the quantitative helicity measurements. The helicity measurements reflect the chain conformation in this case because θ_0 and ϕ_0 are fixed. It was found that K^* is related to helicity via the following equation (Figure 9a)

$$h = 1 - \exp(-0.1K^*) \tag{8}$$

In other words, we can utilize eq 8 to select an appropriate parameter K^* necessary to simulate a chain with a certain helicity, if similar data were to become available through experimental measurements.

https://doi.org/10.1021/acs.macromol.2c00613
Macromolecules 2022, 55, 6321–6331

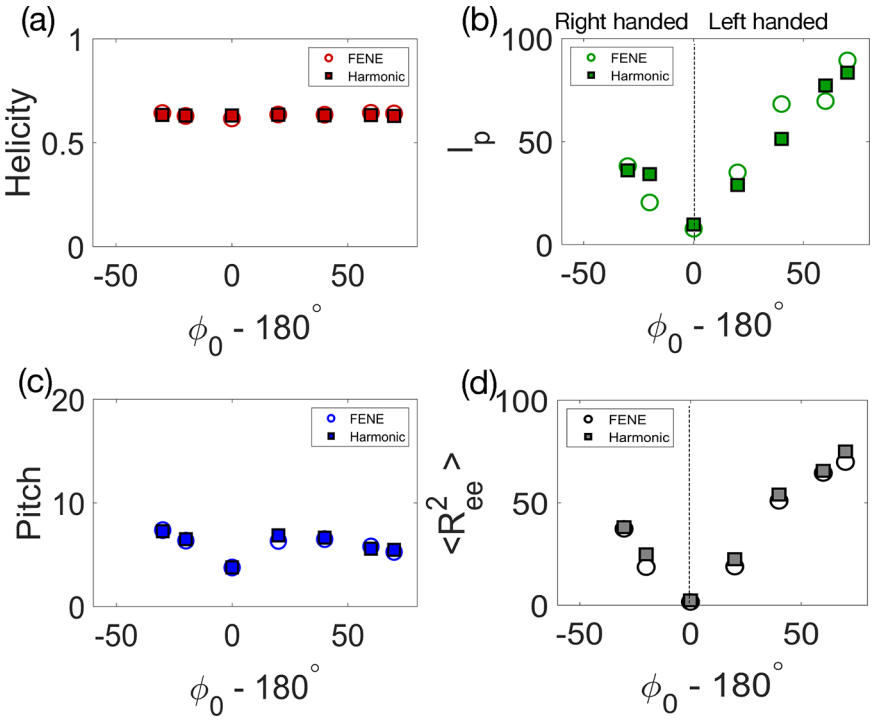

Figure 8. Chain characterization changing with ϕ_0 for K^* = 10: (a) helicity, (b) persistence length, (c) pitch, and (d) mean-square end-to-end distance normalized over N. Results from using the FENE model for bonds are marked with circles, and results from harmonic bonds are marked with squares.

Table 2. Dihedral Set Point ϕ_0 − 180° vs Average Number of Monomers per Helical Turn for Left-Handed Helices

	no. of monomers $\langle s_p \rangle$	
set point ϕ_0 − 180° (deg)	FENE	harmonic
0	13.28	13.30
20	11.24	11.23
40	7.41	7.30
60	5.75	5.30
70	5.00	5.00

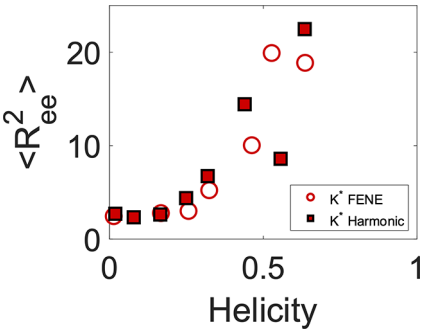

Figure 10. Mean-square end-to-end distance normalized over N increases as helicity is increased when K^* is varied.

Because K^* is the energetic parameter that enforces greater conformity of angles and dihedrals to the set points, a higher value of K^* results in a more structured helix. One expects to see this reflected not only in the increased helicity values (Figure 9a) but also in the mean-square end-to-end distance and persistence lengths. To demonstrate this, the correlations between normalized mean-square end-to-end distance and average helicity are plotted in Figure 10. The correlation between persistence length and helicity is similar but is not presented here. At low values of K^*, the chain behaves more like a random coil, resulting in low helicity, persistence lengths, and $\langle R_{ee}^2 \rangle$. The end-to-end distance is rather independent of

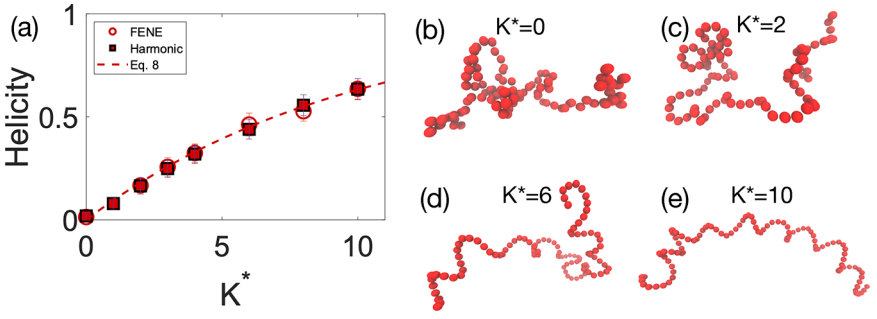

Figure 9. Helicity changing as K^* increases. (a) Average helicity for the last 10% of timesteps fit to the exponential function $h = 1-\exp(-0.1K^*)$. (b–e) Snapshots at select values of K^* with FENE bonds.

https://doi.org/10.1021/acs.macromol.2c00613
Macromolecules 2022, 55, 6321−6331

helicity when helicity is below 0.3. At higher K^*, the chain is more extended and less likely to fold in on itself. In other words, the helical chain exhibits more rodlike behavior which is indicative of high persistence lengths and increased $\langle R_{ee}{}^2 \rangle$.

Parameter Matching to Available Experimental Data. Our next aim is to correlate the model parameters to available experimental data on chiral polymers. The most widely available conformational data for chiral polymers is the persistence length for the chiral polymer and racemic polymer.[20,38,46] In our simulations $K^* = 0$ is considered the reference random coil polymer while a higher value of K^* is necessary for chiral conformations. We can fit the persistence length data from the previous sections (set points $\theta_0 = 160°$ and $\phi_0 - 180° = 20°$, harmonic bonds) to find the correlation between persistence length and K^* over the entire range $0 \leq K^* \leq 10$:

$$\frac{l_{p,\text{helix}}}{l_{p,\text{coil}}} \approx \exp(0.26K^*) \tag{9}$$

Equation 9 may be linearized over a smaller range of $0 \leq K^* \leq 3$. In the absence of additional conformational data from experiments, one must assume some set points θ_0 and ϕ_0 to estimate the desired K^* to model the polymers.

More detailed conformational statistics available for helical and nonhelical polypeptoids in solution[20,38,46] enable further tuning of the simulation parameters. The side groups in the helical molecules had homochiral side groups,[20,38] while the nonhelical molecules had a racemic mixture of the same side chains. Experimental data for a 36-mer glycine-substituted molecule polypeptoid[38] suggested a persistence length ratio of $\frac{l_{p,\text{helix}}}{l_{p,\text{coil}}} = \frac{1.12\text{ nm}}{0.56\text{ nm}} = 2.06$. Yu et al.[20] studied polymers with 60 residues and found that the persistence length of the helical coil was $l_{p,\text{helix}} = 10.5$ Å while the unstructured coil had a persistence length of $l_{p,\text{coil}} = 6.2$ Å, resulting in $\frac{l_{p,\text{helix}}}{l_{p,\text{coil}}} = 1.69$. In addition, the authors estimated 12 jointed helical segments in the chain based on their calculations of persistence length and contour length, which would map on to our variable s_l.[20] Armand et al.[46] noted that the polypeptoid helices are stabilized by steric interactions rather than hydrogen bonds and estimated the molecule to have three peptoids per helical turn, which would map onto $s_p = 3$. On the basis of the available data for polypeptoids, one should be able to select θ_0, ϕ_0, and K^* that would recover the experimental values.

Our approach begins with selecting θ_0 and ϕ_0 since the number of monomers per helical turn (s_p) is largely unaffected by increases in K^* (data not shown). By assuming that one monomer correlates to one simulation bead, we can choose set points to match experimental found values for $s_p \approx 3$ and $s_l = 60/12 \approx 5$.[20] Finally, by adjusting K^*, we can obtain the precise value of the ratio of persistence lengths $l_{p,\text{helix}}/l_{p,\text{coil}} = 1.69$. In Figure 11, we plotted the number of monomers per helical turn, s_p, by varying θ_0 and ϕ_0 for $K^* = 10$. From the data, a narrow band of set points were identified as $80° \leq \theta_0 \leq 100°$ and $220° \leq \phi_0 \leq 240°$ for $s_p \approx 3$.

We then used eq 9 to estimate a value of $K^* = 2.15$ that will produce the desired persistence length ratio. Therefore, for our polypeptoid model, we recalculate our conformational statistics for $1 \leq K^* \leq 3$ and tabulate the results in Table 3.

All parameters sets tested result in values of s_p between 3 and 4, which supports our earlier assertion that this value is largely unaffected by variations in K^*. It also validates our ranges for θ_0 and ϕ_0 values. The greatest amount of variation occurs in s_l which increases as K^* increases. To get $s_l \approx 5$ in this case, we find that $K^* < 3$. The majority of the remaining simulations with $K^* = 2$ nearly match the experimental value for persistence length ratio of 1.69, giving four pairs of set points that closely match the experimental polypeptoid system. The snapshot for $\theta_0 = 80°$, $\phi_0 - 180° = 60°$, and $K^* = 2$ is shown in Figure 11b. Upon comparison of snapshots in Figures 11b and 9c, it is apparent that the set points drastically change the conformation. Thus, to accurately model experimental systems, data on pitch and persistence length are essential.

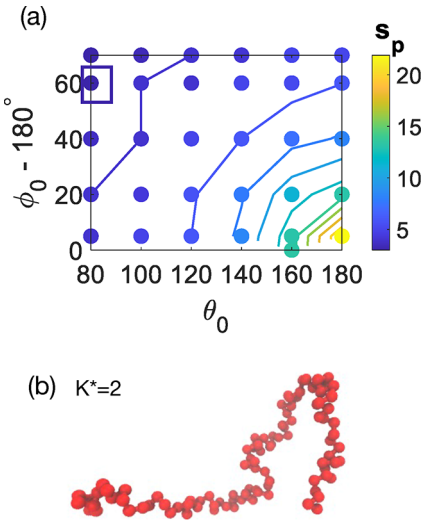

Figure 11. (a) Number of monomers it takes to complete one helical turn (s_p) at different values of θ_0 and ϕ_0 with $K^* = 10$. (b) Snapshot of the chain with $\phi_0 - 180° = 60°$, $\theta_0 = 80°$, and $K^* = 2$.

Table 3. Conformation Measurements for the Set Point Ranges Determined for the Experimental Polypeptoids

set points			conformation measurements		
$\phi_0 - 180°$ (deg)	θ_0 (deg)	K^*	$\langle s_p \rangle$	$\langle s_l \rangle$	$l_{p,\text{helix}}/l_{p,\text{coil}}$
40	80	1	3.533	4.097	1.254
40	80	2	3.867	7.205	1.701
40	80	3	3.767	10.788	2.181
40	100	1	3.933	5.521	1.530
40	100	2	4	6.295	1.600
40	100	3	4	9.839	2.157
60	80	1	3.133	5.517	1.524
60	80	2	3.1	7.106	1.788
60	80	3	3	7.392	1.776
60	100	1	3.567	5.366	1.555
60	100	2	3.767	6.337	1.718
60	100	3	3.967	8.952	2.256

We now turn to the polypeptide-based polymers for which some experimental conformation metrics are available for the polystyrene-*b*-poly(L-lactide), where PS is the achiral block while PLLA is chiral. Yang et al.[47] found the ratio of the Kuhn lengths to be $\frac{b_{\text{PLLA}}}{b_{\text{PS}}} = \frac{12.7\text{ Å}}{6.8\text{ Å}} = 1.89$, which is also the ratio of persistence lengths. Spectroscopic measurements on crystalline PLLA[48] suggest that the number of monomers per helical turn is between 3 and 3.33. On the basis of these values, the simulation parameters for the polypeptide model could be in the similar range as that of the polypeptoid models. However,

https://doi.org/10.1021/acs.macromol.2c00613
Macromolecules 2022, 55, 6321−6331

because the sources of the data were obtained under different thermodynamic conditions (melt and crystalline), the interpretation may not be accurate for the melt or solution state. Additionally, without an estimate of s_l, it is challenging to narrow down the selection of parameters from Table 3. Nevertheless, we note that for what can be considered an inaccurate pair of set points ($\theta_0 = 160°$ and $\phi_0 - 180° = 20°$), eq 9 predicts $K^* = 2.45$, which appears to be well within the range of K^* listed in Table 3.

Overall, on the basis of availability of experimental conformational measurements, we can select values for the set points θ_0 and ϕ_0 and the strength K^*. If only persistence length data are available, assumptions about the set points can be made, and a value of K^* can be obtained that matches the persistence length ratio. Additionally, if the number of monomers per helical turn (s_p) and the number of monomers per rodlike segment (s_l) are available, then those can be used to inform a specific choice of set points. Finally, the parameter K^* can further be used to tune the persistence length. From existing data for chiral polymers, it appears that $K^* = 2-3$ is an appropriate range, suggesting that the molecules neither are very stiff (Figures 9c and 11b) nor have precise helical turns throughout the chain; rather, the molecule exhibits some regions of well-defined helical turns and other floppy regions.

CONCLUSIONS

We have developed a tunable, particle-based, coarse-grained model of a helical polymer chain, capable of exhibiting a wide range of conformations relevant to the self-assembly of chiral block copolymers. Helical conformations are introduced by incorporating an angular and a dihedral potential to the standard Kremer−Grest model. The three tunable parameters are the energetic parameters in the angular and dihedral potentials (set equal to each other) denoted by K, the angular set point θ_0, and the dihedral set point $\phi_0 - 180°$. The resulting conformations are characterized by using helicity (fraction of residues close to the set points), pitch of the helical turn, persistence length, and end-to-end distance.

The pitch of the helix can be increased by increasing the angular set point, θ_0, which also increases the number of monomers in a full helical turn. The handedness of the conformation (left-handed or right-handed) can be controlled by using the dihedral set point, ϕ_0. Values below 180° result in right-handed conformations, and values above 180° result in left-handed conformations. When $|\phi_0 - 180°|$ is increased, the resulting persistence length increases and the number of monomers per turn decreases, while the pitch is fairly constant. Both θ_0 and $|\phi_0 - 180°|$ affect the end-to-end distance where the chain becomes more extended for higher values. The overall structure, measured by the helicity, is controlled with $K^* = K/k_BT$. When $K^* = 0$, the angle and dihedral set points have no effect on the chain, resulting in a random coil polymer. As K^* increases, the chain gains the structure of an ideal helical chain. End-to-end distance correlates with other conformational metrics (pitch, persistence length, and helicity).

Quantitative relationships between model parameters and conformational metrics were also obtained in this work. These are helpful in matching the conformations from the simulation model to experimentally reported measurements. A value of $K^* \approx 2-3$ appears to capture the behavior of both the polypeptoid-based and polypeptide-based chiral polymers, resulting in low helicities. The molecule has some regions with helical turns but also other regions that appear coil-like. Additional selection of appropriate angular and dihedral set points can be made when conformational data on monomers per turn and monomers in a stiff segment is available, as is the case for some of the experimental polypeptoid chemistries. We hope that this work motivates additional experimental characterization of the conformational metrics, particularly for some of the polypeptides. The precisely matched particle-based model can be used in future studies to simulate the melt of block copolymers and decouple intrachain, interchain, and entropic contributions during self-assembly. The model could further be extended to include variations within sequence within the chiral block by changing the set points along the chain.

AUTHOR INFORMATION

Corresponding Author

Poornima Padmanabhan − *Department of Chemical Engineering, Rochester Institute of Technology, Rochester, New York 14623, United States;* orcid.org/0000-0001-9445-1723; Phone: +1 5854754877; Email: poornima.padmanabhan@rit.edu

Authors

Natalie Buchanan − *Department of Chemical Engineering, Rochester Institute of Technology, Rochester, New York 14623, United States; Department of Microsystems Engineering, Rochester Institute of Technology, Rochester, New York 14623, United States*

Joules Provenzano − *Department of Chemical Engineering, Rochester Institute of Technology, Rochester, New York 14623, United States*

Complete contact information is available at: https://pubs.acs.org/10.1021/acs.macromol.2c00613

Notes

The authors declare no competing financial interest.

ACKNOWLEDGMENTS

The authors thank the National Science Foundation DMR-2144511 and the Kate Gleason College Fund for funding support. The authors also thank Research Computing at RIT for computational resources and support in compiling and managing software libraries utilized in this work.

REFERENCES

(1) Yashima, E.; Ousaka, N.; Taura, D.; Shimomura, K.; Ikai, T.; Maeda, K. Supramolecular Helical Systems: Helical Assemblies of Small Molecules, Foldamers, and Polymers with Chiral Amplification and Their Functions. *Chem. Rev.* **2016**, *116*, 13752−13990.

(2) Scanga, R. A.; Reuther, J. F. Helical polymer self-assembly and chiral nanostructure formation. *Polym. Chem.* **2021**, *12*, 1857−1897.

(3) Xia, Q.; Meng, L.; He, T.; Huang, G.; Li, B. S.; Tang, B. Z. Direct Visualization of Chiral Amplification of Chiral Aggregation Induced Emission Molecules in Nematic Liquid Crystals. *ACS Nano* **2021**, *15*, 4956−4966.

(4) Azeroual, S.; Surprenant, J.; Lazzara, T. D.; Kocun, M.; Tao, Y.; Cuccia, L. A.; Lehn, J.-M. Mirror symmetry breaking and chiral amplification in foldamer-based supramolecular helical aggregates. *Chem. Commun.* **2012**, *48*, 2292−2294.

(5) Anderson, T. W.; Sanders, J. K. M.; Pantoş, G. D. The sergeants-and-soldiers effect: chiral amplification in naphthalenediimide nanotubes. *Org. Biomol. Chem.* **2010**, *8*, 4274−4280.

(6) Saranathan, V.; Osuji, C.; Mochrie, S.; Noh, H.; Narayanan, S.; Dufresne, E.; Sandy, A.; Prum, R. Structure, function, and self-

assembly of single network gyroid (I4 132) photonic crystals in butterfly wing scales. *Proc. Natl. Acad. Sci. U. S. A.* **2010**, *107*, 11676−11681.
(7) Winter, B.; Butz, B.; Dieker, C.; Schröder-Turk, G. E.; Mecke, K.; Spiecker, E. Coexistence of both gyroid chiralities in individual butterfly wing scales of Callophrys rubi. *Proc. Natl. Acad. Sci. U. S. A.* **2015**, *112*, 12911−6.
(8) Mille, C.; Tyrode, E. C.; Corkery, R. W. 3D titania photonic crystals replicated from gyroid structures in butterfly wing scales: Approaching full band gaps at visible wavelengths. *RSC Adv.* **2013**, *3*, 3109−3117.
(9) Corkery, R. W.; Tyrode, E. C. On the colour of wing scales in butterflies: Iridescence and preferred orientation of single gyroid photonic crystals. *Interface Focus* **2017**, *7*, 20160154.
(10) Wang, H. F.; Chiu, P. T.; Yang, C. Y.; Xie, Z. H.; Hung, Y. C.; Lee, J. Y.; Tsai, J. C.; Prasad, I.; Jinnai, H.; Thomas, E. L.; Ho, R. M. Networks with controlled chirality via self-assembly of chiral triblock terpolymers. *Science Advances* **2020**, DOI: 10.1126/sciadv.abc3644.
(11) Ho, R. M.; Chiang, Y. W.; Chen, C. K.; Wang, H. W.; Hasegawa, H.; Akasaka, S.; Thomas, E. L.; Burger, C.; Hsiao, B. S. Block copolymers with a twist. *J. Am. Chem. Soc.* **2009**, *131*, 18533−18542.
(12) Chen, C. K.; Hsueh, H. Y.; Chiang, Y. W.; Ho, R. M.; Akasaka, S.; Hasegawa, H. Single helix to double gyroid in chiral block copolymers. *Macromolecules* **2010**, *43*, 8637−8644.
(13) Wang, H. F.; Wang, H. W.; Ho, R. M. Helical phase from blending of chiral block copolymer and homopolymer. *Chem. Commun.* **2012**, *48*, 3665−3667.
(14) Zhao, W.; Liu, F.; Wei, X.; Chen, D.; Grason, G. M.; Russell, T. P. Formation of H* phase in chiral block copolymers: Morphology evolution as revealed by time-resolved X-ray scattering. *Macromolecules* **2013**, *46*, 474−483.
(15) Wen, T.; Wang, H. F.; Li, M. C.; Ho, R. M. Homochiral Evolution in Self-Assembled Chiral Polymers and Block Copolymers. *Acc. Chem. Res.* **2017**, *50*, 1011−1021.
(16) Higuchi, T.; Sugimori, H.; Jiang, X.; Hong, S.; Matsunaga, K.; Kaneko, T.; Abetz, V.; Takahara, A.; Jinnai, H. Morphological Control of Helical Structures of an ABC-Type Triblock Terpolymer by Distribution Control of a Blending Homopolymer in a Block Copolymer Microdomain. *Macromolecules* **2013**, *46*, 6991−6997.
(17) Yang, K. C.; Ho, R. M. Spiral Hierarchical Superstructures from Twisted Ribbons of Self-Assembled Chiral Block Copolymers. *ACS Macro Lett.* **2020**, *9*, 1130−1134.
(18) Murnen, H. K.; Rosales, A. M.; Jaworski, J. N.; Segalman, R. A.; Zuckermann, R. N. Hierarchical self-assembly of a biomimetic diblock copolypeptoid into homochiral superhelices. *J. Am. Chem. Soc.* **2010**, *132*, 16112−16119.
(19) Xu, P.; Gao, L.; Cai, C.; Lin, J.; Wang, L.; Tian, X. Helical Toroids Self-Assembled from a Binary System of Polypeptide Homopolymer and its Block Copolymer. *Angew. Chem., Int. Ed.* **2020**, *59*, 14281−14285.
(20) Yu, B.; Danielsen, S. P.; Patterson, A. L.; Davidson, E. C.; Segalman, R. A. Effects of Helical Chain Shape on Lamellae-Forming Block Copolymer Self-Assembly. *Macromolecules* **2019**, *52*, 2560−2568.
(21) Davidson, E. C.; Rosales, A. M.; Patterson, A. L.; Russ, B.; Yu, B.; Zuckermann, R. N.; Segalman, R. A. Impact of Helical Chain Shape in Sequence-Defined Polymers on Polypeptoid Block Copolymer Self-Assembly. *Macromolecules* **2018**, *51*, 2089−2098.
(22) Yu, B.; Li, R.; Segalman, R. A. Tuning the Double Gyroid Phase Window in Block Copolymers via Polymer Chain Conformation Near the Interface. *Macromolecules* **2021**, *54*, 5388−5396.
(23) Zhao, W.; Russell, T. P.; Grason, G. M. Orientational interactions in block copolymer melts: Self-consistent field theory. *J. Chem. Phys.* **2012**, *137*, 104911.
(24) Zhao, W.; Russell, T. P.; Grason, G. M. Chirality in block copolymer melts: Mesoscopic helicity from intersegment twist. *Phys. Rev. Lett.* **2013**, *110*, 1−5.
(25) Grason, G. M. Chirality transfer in block copolymer melts: Emerging concepts. *ACS Macro Lett.* **2015**, *4*, 526−532.
(26) Nanda, V.; DeGrado, W. F. Simulated evolution of emergent chiral structures in polyalanine. *J. Am. Chem. Soc.* **2004**, *126*, 14459−14467.
(27) Zerze, G. H.; Khan, M. N.; Stillinger, F. H.; Debenedetti, P. G. Computational Investigation of the Effect of Backbone Chiral Inversions on Polypeptide Structure. *J. Phys. Chem. B* **2018**, *122*, 6357−6363.
(28) MacKerell, Jr., A. D.; Brooks, B.; Brooks, III, C. L.; Nilsson, L.; Roux, B.; Won, Y.; Karplus, M. CHARMM: The Energy Function and Its Parameterization. In *Encyclopedia of Computational Chemistry*; John Wiley & Sons, Ltd.: 2002.
(29) Marrink, S. J.; Risselada, H. J.; Yefimov, S.; Tieleman, D. P.; De Vries, A. H. The MARTINI force field: Coarse grained model for biomolecular simulations. *J. Phys. Chem. B* **2007**, *111*, 7812−7824.
(30) Ingólfsson, H. I.; Lopez, C. A.; Uusitalo, J. J.; de Jong, D. H.; Gopal, S. M.; Periole, X.; Marrink, S. J. The power of coarse graining in biomolecular simulations. *Wiley Interdisciplinary Reviews: Computational Molecular Science* **2014**, *4*, 225−248.
(31) Zimm, B. H.; Bragg, J. K. Theory of the Phase Transition between Helix and Random Coil in Polypeptide Chains. *J. Chem. Phys.* **1959**, *31*, 526−535.
(32) Kemp, J. P.; Chen, Z. Y. Formation of Helical States in Wormlike Polymer Chains. *Phys. Rev. Lett.* **1998**, *81*, 3880−3883.
(33) Varshney, V.; Dirama, T. E.; Sen, T. Z.; Carri, G. A. A minimal model for the helix-coil transition of wormlike polymers. Insights from Monte Carlo simulations and theoretical implications. *Macromolecules* **2004**, *37*, 8794−8804.
(34) Boehm, C. R.; Terentjev, E. M. Minimal Model of Intrinsic Chirality to Study the Folding Behavior of Helical Polymers. *Macromolecules* **2014**, *47*, 6086−6094.
(35) Williams, M. J.; Bachmann, M. System-size dependence of helix-bundle formation for generic semiflexible polymers. *Polymers* **2016**, *8*, 1−13.
(36) Liu, Y.; Pérez, T.; Li, W.; Gunton, J. D.; Green, A. Statistical mechanics of helical wormlike chain model. *J. Chem. Phys.* **2011**, *134*, 065107.
(37) Yamakawa, H.; Yoshizaki, T. *Helical Wormlike Chains in Polymer Solutions*; Springer: Berlin, 2016; pp 1−511.
(38) Rosales, A. M.; Murnen, H. K.; Kline, S. R.; Zuckermann, R. N.; Segalman, R. A. Determination of the persistence length of helical and non-helical polypeptoids in solution. *Soft Matter* **2012**, *8*, 3673−3680.
(39) Plimpton, S. Fast Parallel Algorithms for Short-Range Molecular Dynamics. *J. Comput. Phys.* **1995**, *117*, 1−19.
(40) Rochester Institute of Technology *Research Computing Services*, 2019; https://www.rit.edu/researchcomputing/.
(41) Kremer, K.; Grest, G. S. Dynamics of entangled linear polymer melts: A molecular-dynamics simulation. *J. Chem. Phys.* **1990**, *92*, 5057−5086.
(42) Jones, J. On the determination of molecular fields.—I. From the variation of the viscosity of a gas with temperature. *Proc. R. Soc. London. Series A, Containing Papers of a Mathematical and Physical Character* **1924**, *106*, 441−462.
(43) Weeks, J. D.; Chandler, D.; Andersen, H. C. Role of Repulsive Forces in Determining the Equilibrium Structure of Simple Liquids. *J. Chem. Phys.* **1971**, *54*, 5237−5247.
(44) Kozuch, D. J.; Zhang, W.; Milner, S. T. Predicting the Flory-Huggins χ parameter for polymers with stiffness mismatch from molecular dynamics simulations. *Polymers* **2016**, *8*, 241.
(45) Hansmann, U. H. E.; Okamoto, Y. Finite-size scaling of helix−coil transitions in poly-alanine studied by multicanonical simulations. *J. Chem. Phys.* **1999**, *110*, 1267−1276.
(46) Armand, P.; Kirshenbaum, K.; Goldsmith, R. A.; Farr-Jones, S.; Barron, A. E.; Truong, K. T. V.; Dill, K. A.; Mierke, D. F.; Cohen, F. E.; Zuckermann, R. N.; Bradley, E. K. NMR determination of the major solution conformation of a peptoid pentamer with chiral side chains. *Proc. Natl. Acad. Sci. U. S. A.* **1998**, *95*, 4309−4314.

(47) Yang, K. C.; Chiu, P. T.; Tsai, H. W.; Ho, R. M. Self-Assembly of Semiflexible-Coil Chiral Block Copolymers under Various Segregation Strengths with Multiple Secondary Interactions. *Macromolecules* **2021**, *54*, 9850−9859.
(48) Kang, S.; Hsu, S. L.; Stidham, H. D.; Smith, P. B.; Leugers, M. A.; Yang, X. A Spectroscopic Analysis of Poly(lactic acid) Structure. *Macromolecules* **2001**, *34*, 4542−4548.

https://doi.org/10.1021/acs.macromol.2c00613
Macromolecules 2022, 55, 6321−6331